ACS APPLIED MATERIALS & INTERFACES

Research Article

www.acsami.org

Using an Airbrush Pen for Layer-by-Layer Growth of Continuous Perovskite Thin Films for Hybrid Solar Cells

Mohan Ramesh,[†] Karunakara Moorthy Boopathi,[†,‡,§] Tzu-Yen Huang,[†,∥] Yu-Ching Huang,[⊥] Cheng-Si Tsao,[⊥] and Chih-Wei Chu*[,†]

[†]Research Center for Applied Sciences, Academia Sinica, Taipei 115, Taiwan R.O.C.

[‡]Nanoscience and Technology Program, Taiwan International Graduate Program, Academia Sinica and National Tsing Hua University,Taiwan R.O.C.

[§]Department of Engineering and Systems Science, National Tsing Hua University, Hsinchu 30013, Taiwan R.O.C.

[∥]Department of Chemical Engineering, National Taiwan University, Taipei 10617, Taiwan R.O.C.

[⊥]Institute of Nuclear Energy Research, Longtan, Taoyuan 32546, Taiwan R.O.C.

Supporting Information

ABSTRACT: In this manuscript we describe hybrid heterojunction solar cells, having the device architecture glass/indium tin oxide/poly(3,4-ethylenedioxythiopene)/poly(styrenesulfonic acid)/perovskite/[6,6]-phenyl-C_{61}-butyric acid methyl ester/C_{60}/2,9-dimethyl- 4,7-diphenyl-1,10-phenanthroline/Al, fabricated using lead halide perovskite obtained through spray-coating at a low precursor concentration. To study the relationship between the morphology and device performance, we recorded scanning electron microscopy images of perovskite films prepared at various precursor ratios, spray volumes, substrate temperatures, and postspray annealing temperatures. Optimization of the spray conditions ensured uniform film growth and high surface area coverage at low substrate temperatures. Lead halide perovskite solar cells prepared under the optimal conditions displayed an average power conversion efficiency (PCE) of approximately 9.2%, with 85% of such devices having efficiencies of greater than 8.3%. The best-performing device exhibited a short-circuit current density of 17.3 mA cm^{-2}, a fill factor of 0.63, and an open-circuit voltage of 0.93 V, resulting in a PCE of 10.2%. Because spray-coating technology allows large-area deposition, we also fabricated devices having areas of 60 and 342 mm^2, achieving PCEs with these devices of 6.88 and 4.66%, respectively.

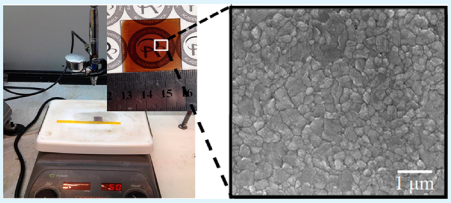

KEYWORDS: *perovskite, hybrid solar cells, spray-coating, solution process, large area, low temperatures*

INTRODUCTION

Solution-processing methods, including spin-coating, spraying, blade-coating, and screen printing, are cheap means of fabricating thin-film solar cells.[1,2] For example, a device exhibiting a power conversion efficiency (PCE) of 10% has been achieved through use of a solution-processed metal chalcogenide that had been subjected to a high-temperature sintering process.[3,4] Similarly, dye-sensitized and organic photovoltaic (PV) devices having PCEs of greater than 8% have also been developed through the synthesis of novel small molecules and polymers.[5−8] Although thin-film solar cells can be fabricated by employing facile solution processing, the efficiencies of such devices remain far behind those of Si-based counterparts. Organometal halide perovskites (ABX_3), comprising a cation A sealed with a small-molecule species [methylammonium iodide (MAI), CH_3NH_3I] and a network of corner-sharing BX6 octahedra (where the metal cation B is Sn^{2+} or Pb^{2+} and the halide X is typically F^-, Cl^-, Br^-, or I^-), are a common class of semiconductors. Recently, mixed-halide perovskites have displayed electron−hole diffusion lengths of greater than 1 μm, with high charge-carrier mobilities and bipolar transport behavior.[9] Accordingly, perovskite compounds based on organometal halides have become innovative alternatives for next-generation PV devices. Indeed, devices based on mesoporous or planar heterojunction structures have exhibited attractive PCEs as high as 15%.[10−15] Such high efficiencies, combined with solution processing, suggest that perovskite materials have great potential for use in fabricating inexpensive, large-area solar cells.

Although great progress has been made in the development of hybrid architectures featuring an n-TiO_2/perovskite/hole transporting layer, the stability of such devices has remained poor upon continuous exposure to light.[16] Moreover, obtaining a high-quality condensed TiO_2 layer requires high-temperature treatment (ca. 450 °C), which limits preparation on flexible substrates. To fabricate stable perovskite solar cells with processing at low temperatures, a thin layer of poly(3,4-ethylenedioxythiopene):poly(styrenesulfonic acid) (PEDOT:PSS) and PCBM can be used as the hole transport layer and electron transport layer when building a planar heterojunction perovskite solar cell [indium tin oxide (ITO)/PEDOT:PSS/perovskite/PCBM].[17−22] Because of rapid crys-

Received: October 7, 2014
Accepted: January 6, 2015
Published: January 6, 2015

DOI: 10.1021/am506886d
ACS Appl. Mater. Interfaces 2015, 7, 2359−2366

tallization, however, some difficulties are encountered when attempting to fabricate perovskite materials as thermodynamically stable thin films on PEDOT:PSS surfaces. Dewetting or agglomeration can result in incomplete coverage and a nonuniform film thickness after solution processing and subsequent baking. The voids/pores in perovskite films will minimize the open-circuit voltage (V_{OC}) and fill factor (FF) by creating paths for a low shunt resistance (R_{sh}) and a high series resistance (R_s) between the electrodes of the solar cell. Moreover, high material wastage from spin-coating can increase the cost of the materials used for fabrication over a large area.[23] To push this technology to the real market, we must develop methods for fabrication over large areas with low material wastage. Several existing large-area coating methods (e.g., blade coating, spraying, printing, slot-die coating) are compatible with the high-speed, high-volume, low-cost, roll-to-roll methods of production envisioned for commercialization. Accordingly, studies of perovskite film formation through each of these techniques are of relevance. Recently, Lidzey et al. reported a mixed halide perovskite film having an 85% area coverage prepared through ultrasonic vibrating spray-deposition, and resulting devices exhibiting average PCEs of 4−8%.[24] Thus, spray deposition appears to be a promising technique for fabricating large-area perovskite solar cells.

In this manuscript, we report how a normal airbrush pen can be used in the fabrication of continuous methylammonium lead(II) iodide perovskite films for efficient solar cells. We optimized the performance of such devices through variations in the precursor ratios, the substrate temperature, the postspray annealing temperature, and the thickness of the perovskite film. The device exhibiting the best performance featured almost 100% film coverage, with preparation at a substrate temperature of 50 °C and a postspray annealing temperature of 100 °C. The average device exhibited a PCE of 9.2%, with the champion cell displaying a PCE of 10.2%. By taking advantage of spray-coating, we demonstrated the preparation of large-area devices with promising efficiencies.

EXPERIMENTAL SECTION

Preparation of Methylammonium Iodide. MAI powder was synthesized following the method described by Wang et al.[25] Concentrated aqueous hydroiodic acid (HI; 57 wt % in water, Alfa Aesar; 15.0 mL) was reacted with methylamine (CH_3NH_2; 40 wt % in aqueous solution; 13.5 mL) in a three-neck flask at 0 °C (ice bath) for 2 h with constant stirring under a N_2 atmosphere. MAI crystallized upon rotary evaporation of the solvent. The generated white powder was collected after washing three times with Et_2O and drying under vacuum at 60 °C overnight. The dried powder was stored in a glovebox until required for further use.

Device Fabrication and Characterization. ITO-coated glass substrates (<10 Ω sq^{-1}, RiTdisplay) were cleaned through sonication, once in detergent (20 min), twice in deionized (DI) water (20 min each), and then dried under a stream of N_2. The substrates were treated with UV light and ozone for 15 min to clean the surfaces and also to improve the surface adhesion. PEDOT:PSS was spin-coated (4000 rpm) onto the ITO surfaces for 1 min, followed by annealing at 130 °C for 30 min. The substrates were transferred to a glovebox for spray-coating of the perovskite active layer. The precursors MAI and PbI_2 (99%, Alfa Aesar) were dissolved in anhydrous *N*,*N*-dimethylformamide (DMF) at various molar weight ratios (1:0.65, 1:0.7, 1:0.75, 1:0.8, and 1:1) at a concentration of approximately 1 wt %. Each mixed solution was stirred on a hot plate at 70 °C overnight. The mixed solutions of various weight ratios were spray-coated onto the PEDOT:PSS film at a substrate temperature of 50 °C by using a normal airbrush pen [Figure 1a]. After spraying, the sample was kept on the hot plate at 100 °C for 60 min to form a crystalline perovskite film. A solution (20 mg/mL) of PCBM (85 nm) in chlorobenzene (CB) was spun (6000 rpm, 60 s) onto the perovskite layer, followed by annealing at 90 °C for 30 min. The device structure was completed through sequential thermal evaporation of C_{60} (30 nm), 2,9-dimethyl-4,7-diphenyl-1,10-phenanthroline (BCP, 7 nm), and an aluminum electrode (100 nm) through a shadow mask under vacuum (pressure: 1×10^{-6} Torr). The active area of each device was 10 mm^2.

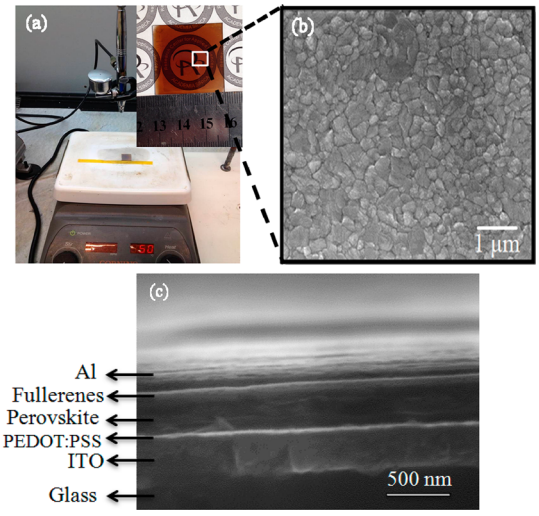

Figure 1. (a) Photograph of the spray-coating setup for a large-area device. (b) Top-view SEM image of a spray-coated perovskite film on a ITO/PEDOT:PSS substrate. (c) Cross-sectional SEM image of the photovoltaic device architecture (glass/ITO/PEDOT:PSS/perovskite/PCBM/C_{60}/BCP/Al).

Powder X-ray diffraction (XRD) patterns were recorded at room temperature (RT) using a Bruker D8 X-ray diffractometer equipped with a diffracted beam monochromator set for Cu Kα radiation (λ = 1.540 56 Å) in the 2θ range of 10−80° with a step size of 0.01655° and step time of 0.4 s. Scanning electron microscopy (SEM) was performed using an FEI Noval 200 scanning electron microscope (15 kV). ITO substrates spin-coated with PEDOT:PSS were used for both XRD and SEM imaging. Photoluminescence (PL) emission spectra of the samples were recorded using an optically excited Q-switched Nd:YAG laser (266 nm, 3−5 ns pulse, 10 Hz) focused to a beam diameter of approximately 0.5 mm. Absorption spectra of films on glass substrates were measured at RT using a Jacobs V-670 UV−vis spectrophotometer. The devices were illuminated with a solar simulator (Thermal Oriel 1000 W), which provided a simulated AM 1.5 spectrum (100 mW cm^{-2}), inside a glovebox, using a Xe lamp. The light intensity was calibrated using a monosilicon photodiode with a KG-5 color filter (Hamamatsu). The solar cells were illuminated under aperture metal mask (0.1 cm^2) to define the active area.

RESULTS AND DISCUSSION

Figure 1a presents the spray-coating setup, comprising an airbrush pen, an air compressor, and a hot plate, which we used to deposit perovskite thin films with low wastage of the MAI and PbI_2 mixed solutions. During perovskite film deposition, the nozzle width and the distance (13 cm) between the nozzle and the substrate were fixed to ensure films of good quality. We could achieve continuous, pinhole-free $MAPbI_3$ films with large area coverage through control over the spray conditions, as revealed in the top-view SEM image in Figure 1b. The cross-sectional SEM image of the full device in Figure 1c further confirms that a continuous, pinhole-free perovskite film had been deposited on the PEDOT:PSS layer.

The optical and electronic properties of perovskite films are very sensitive to their compositions. Accordingly, we recorded

DOI: 10.1021/am506886d
ACS Appl. Mater. Interfaces 2015, 7, 2359−2366

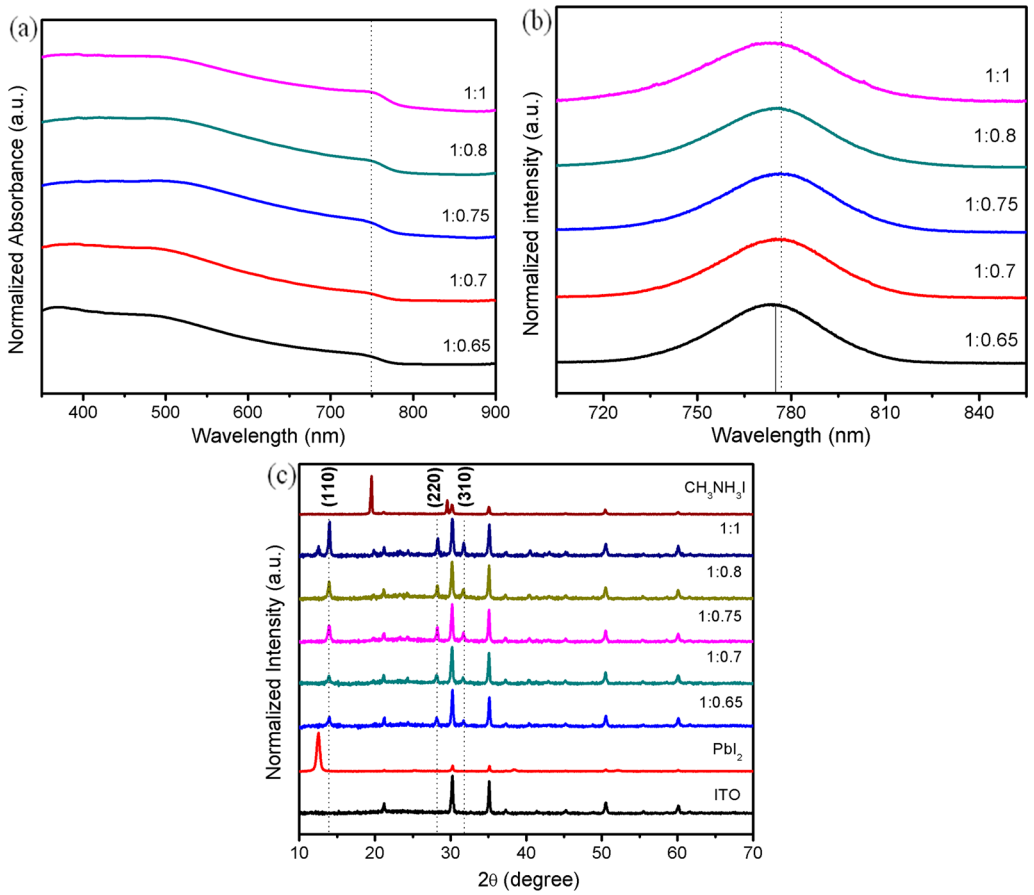

Figure 2. (a, b) Absorption and PL spectra of perovskite films prepared at various MAI/PbI_2 ratios and (c) XRD patterns of PbI2, MAI, and perovskite films prepared at various MAI/PbI_2 ratios; 300 μL of a solution was sprayed onto the ITO/PEDOT:PSS surface at a substrate temperature of 50 °C, followed by annealing at 100 °C for 1 h.

UV−vis and PL spectra and XRD patterns to evaluate the films formed at various MAI/PbI_2 ratios. Figure 2a,b displays typical absorption and PL spectra of the perovskite films at the various precursor ratios. A broad absorption across the UV−vis range and absorption peaks near 743 nm reveal the formation of a perovskite film. Upon elevating the relative PbI_2 content from 0.65 to 1, both the absorption and PL (776 nm) peaks shifted slightly with enhanced intensity.[25,26] To confirm the stoichiometric perovskite formation, we sprayed MAI/PbI_2 mixtures onto ITO/PEDOT:PSS substrates and recorded their XRD patterns. Figure 2c reveals evidence for tetragonal-structured perovskite with signals at values of 2θ of 14.08 (110), 28.5 (220), and 31.8° (310). Stoichiometric film formation was indicated primarily at the value of 2θ of 14.08°, where the signal intensity increased upon increasing the relative ratio of PbI_2 from 0.65 to 1.

Figure 3a presents the typical current density−voltage (J−V) characteristics of the devices prepared with MAI/PbI_2 ratios ranging from 1:0.65 to 1:1. In each case, the volume of the sprayed precursor solution was maintained at 300 μL, PCBM was spun at 6000 rpm, and C_{60} was thermally evaporated to a thickness of approximately 30 nm. The device prepared at an MAI/PbI_2 ratio of 1:0.65 exhibited a low short-circuit current density (J_{SC}) of 11.2 mA cm^{-2}, a value of V_{OC} of 0.76 V, and an FF of 0.49, resulting in a PCE of 4.23 ± 0.2%. The device performance increased slightly upon increasing the MAI/PbI_2 ratio to 1:0.7; it reached a PCE of 9.7 ± 1.5% for the device prepared at an MAI/PbI_2 ratio of 1:0.75, with values of J_{SC}, V_{OC}, and FF of 16.3 mA cm^{-2}, 0.90 V, and 0.65, respectively. To examine the cause of this behavior, Supporting Information, Figure S1 displays the dark current plotted for each of these devices. The leakage current for the device prepared at an MAI/PbI_2 ratio of 1:0.75 was 1 order of magnitude lower than those of the others. Because the leakage current is also related to the morphology, we recorded top-view SEM images for films prepared at each of these ratios. Figure 4a−e presents top-view SEM images of perovskite films prepared from solutions (300 μL), containing various precursor ratios, sprayed onto ITO/PEDOT:PSS substrates while heating at 50 °C, followed immediately by postspray annealing at 100 °C for 1 h. At the lowest MAI/PbI_2 ratio (1:0.65), the film exhibited dewetting and incomplete crystallization, due to the excess of MAI. Increasing the relative PbI_2 content to 0.7 and 0.75 caused the films to become more uniform, by balancing the stoichiometric ratio, with increased wettability, although the grains were smaller in the latter sample. The device incorporating the perovskite film formed at an MAI/PbI_2 ratio of 1:0.75 exhibited a PCE (9.7 ± 1.5%) higher than that of the corresponding device formed at an MAI/PbI_2 ratio of 1:0.7 (6.7 ± 0.8% PCE), consistent with the effect of crystallinity. At an MAI/PbI_2 ratio of 1:0.7, the crystallinity of the perovskite was poorer as a result of unbalanced stoichiometry. Further increasing the MAI/PbI_2 ratio to 1:0.8 and 1:1 caused larger microfiber grains to appear (Figure 4d,e); accordingly, the device performance dropped considerably to PCEs of 5.5 ± 0.55 and 4.78 ± 0.4%, respectively. Table 1 summarizes the performances of the

DOI: 10.1021/am506886d
ACS Appl. Mater. Interfaces 2015, 7, 2359−2366

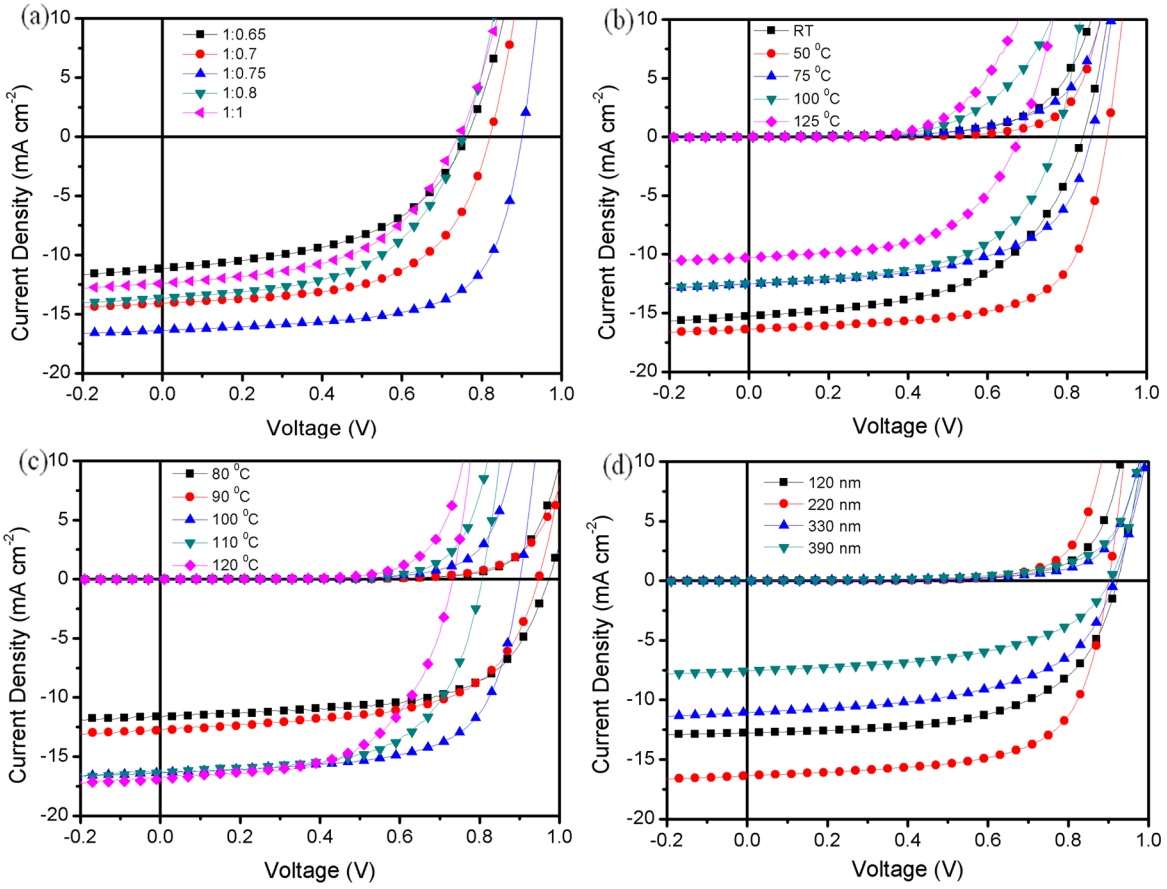

Figure 3. Current density–voltage characteristics of devices incorporating perovskite films prepared at various (a) precursor (MAI/PbI_2) ratios, (b) substrate temperatures, (c) annealing temperatures, and (d) thicknesses.

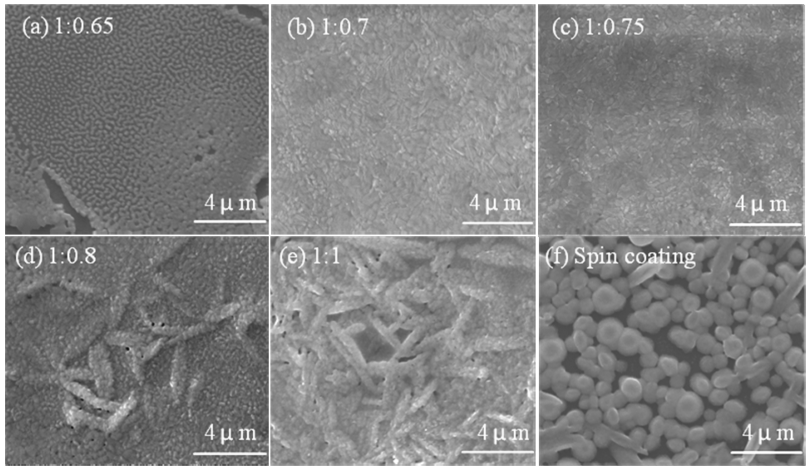

Figure 4. Top-view SEM images of perovskite films prepared through (a–e) spray-coating of precursor solutions (300 μL) containing various MAI/PbI_2 ratios onto ITO/PEDOT:PSS substrates at a substrate temperature of 50 °C, with subsequent annealing at 100 °C for 1 h, and (f) spin-coating of a precursor solution (MAI/PbI_2 ratio = 1:0.75) at 1000 rpm for 45 s and then annealing at 100 °C for 1 h.

devices prepared using the various MAI/PbI_2 ratios. An excess of PbI_2 increased the average grain size and increased the average pore size; this excess remained unreacted at a 1:1 ratio, as evidenced by the presence of the peak at a value of 2θ of 12.5° (Figure 2c).To examine the difference between films prepared through spin-coating and spray-casting, we also recorded an SEM image for a substrate spin-coated from a precursor solution at an MAI/PbI_2 ratio of 1:0.75 (Figure 4f). The morphology of the spin-coated film was nonuniform and discontinuous, with random grain sizes. Larger grain sizes and pinholes, which created paths that decreased the value of R_{sh} and increased the value of R_s, were responsible for the lower values of V_{OC} and FF. The J–V characteristics of our devices incorporating the spray-cast films revealed that the FF reached a maximum value of 0.65 for the sample prepared at a MAI/PbI_2 ratio of 1:0.75, along with the highest value of R_{sh} (813.01) and the lowest value of R_s (3.1).

DOI: 10.1021/am506886d
ACS Appl. Mater. Interfaces 2015, 7, 2359–2366

Table 1. Photovoltaic Performance Parameters of Devices Incorporating Perovskite Films Prepared Using Various Ratios of the MAI/PbI_2 Precursors

MAI/PbI_2 ratio	J_{SC} [mA cm^{-2}]	V_{OC} [mV]	FF	PCE [%]	R_{sh}	R_s
1:0.65	11.2	0.76	0.49	4.23[a] (4.2)[b]	429.19	4.515
1:0.7	14.1	0.81	0.58	6.7[a] (6.4)[b]	595.59	4.28
1:0.75	16.3	0.9	0.65	9.77[a] (9.2)[b]	813.01	3.11
1:0.8	13.6	0.75	0.53	5.5[a] (5.4)[b]	505.05	3.22
1:1	12.4	0.74	0.52	4.78[a] (4.6)[b]	407.51	5.52

[a]Best device performance. [b]Average device performance.

The crystallinity and morphology of each film depended on the dynamics of annealing. To determine the influence of the annealing temperature on the device performance, we examined the effects of different annealing temperatures during and after the spray deposition. We monitored the photocurrents of devices prepared using various substrate temperatures (from RT to 125 °C) during the spraying process, while fixing the postspray annealing temperature at 100 °C (Figure 3b); we also monitored them (Figure 3c) after fixing the substrate temperature at 50 °C and varying the annealing temperature (from 80 to 120 °C). When incorporating a film prepared at a substrate temperature of RT, the device exhibited a J_{SC} value of 15.28 mA cm^{-2}, a V_{OC} value of 0.84 V, and a PCE value of 6.9%; the latter reached its maximum value of 9.7 ± 1.5% when the substrate temperature was 50 °C. Increasing the substrate temperature thereafter, from 75 to 125 °C, decreased the PCE dramatically, as a result of decreases in both J_{SC} and V_{OC}. The effect of the postspray annealing temperature on device performance was reverse. When we increased the annealing temperature of the perovskite film from 80 to 90 °C, the PCE remained at 7% with an increase in the value of J_{SC} from 11.69 to 12.8 mA cm^{-2} and a decrease in the value of V_{OC} from 0.97 to 0.94 V. Further increasing the temperature from 100 to 120 °C caused the value of J_{SC} to increase to greater than 16 mA cm^{-2} and the value of V_{OC} to decrease to less than 0.8 V, with the PCE reaching its highest value for an annealing temperature of 100 °C. Table 2 summarizes the performance data for the devices prepared with various annealing conditions. Supporting Information, Figure S2 presents top-view SEM images of the perovskite films deposited at substrate temperatures from RT to 100 °C during spraying, while maintaining the postspray annealing temperature at 100 °C. For substrate temperatures of RT, 50, and 75 °C, the morphologies appeared similar, although the device performances varied dramatically. We suspect that film packing played an important role affecting the PCE of the resulting devices. Solvent accumulation presumably occurred during continuous spraying at RT, forming an inhomogeneous surface. By increasing the substrate temperature to 50 °C, the film became more homogeneous and had a higher coverage. When the substrate temperature was 75 or 100 °C, however, pores began to appear as a result of rapid evaporation of the solvent. Even though DMF has a high boiling point, the microdroplets that scattered from the nozzle evaporated faster at 75 and 100 °C than they did at 50 °C upon reaching the substrate. The changes in film morphology upon varying the annealing temperature were driven by the surface energy minimization and mass loss;[27] therefore, we investigated the effect of the postspray annealing temperature through analyses of UV−vis spectra, XRD patterns, and SEM images. Supporting Information, Figure S3a displays the UV−vis absorption spectra for the perovskite films prepared at an MAI/PbI_2 ratio of 1:0.75 and various annealing temperatures (from 80 to 120 °C). The peak near 743 nm was absent when the annealing temperature was 80 or 90 °C but appeared at annealing temperatures of 100 °C or above. Corresponding SEM images (Supporting Information, Figure S4) revealed that the films were more homogeneous (smaller pore sizes), but their crystallization was poorer, when annealed at 80 and 90 °C than when annealed at 100 °C (Supporting Information, Figure S3b). Further increasing the annealing temperature to 110 and 120 °C resulted in the perovskite films undergoing partial dewetting with higher crystallinity and larger grain sizes, leading to relatively low surface coverages. Increasing the temperature enhanced the crystallinity of the perovskite films with a corresponding increase in the size of the micrograins.[28]

The thickness of a perovskite film can affect the carrier diffusion length in a device that strongly absorbs light in the red spectral region. Accordingly, we prepared devices in which we varied the thickness of the perovskite film (120, 220, 330, and

Table 2. Photovoltaic Performance Parameters of Devices Incorporating Perovskite Films Prepared at Various Substrate Temperatures, Annealing Temperatures, and Thicknesses

	temperatures (°C)					
thickness of $CH_3NH_3PbI_3$ [nm]	substrate	postspray annealing	J_{SC} [mA cm^{-2}]	V_{OC} [mV]	FF	PCE [%]
220 ± 20	RT	100	15.28	0.84	0.54	6.9[a] (6.7)[b]
	50		16.36	0.90	0.65	9.7[a] (9.2)[b]
	75		12.5	0.86	0.57	6.2[a] (6.1)[b]
	100		12.5	0.77	0.56	5.4[a] (5.3)[b]
	125		10.3	0.69	0.53	3.8[a] (3.7)[b]
220 ± 20	50	80	11.69	0.97	0.61	7[a] (7)[b]
		90	12.8	0.94	0.61	7.2[a] (7.1)[b]
		100	16.36	0.90	0.65	9.7[a] (9.2)[b]
		110	16.2	0.81	0.61	8.1[a] (8.0)[b]
		120	16.8	0.73	0.58	7.2[a] (7)[b]
120 ± 10	50	100	12.77	0.92	0.59	7.03[a] (6.7)[b]
220 ± 20			16.36	0.92	0.65	9.7[a] (9.2)[b]
330 ± 15			11.06	0.91	0.55	5.64[a] (5.51)[b]
390 ± 25			7.50	0.9	0.53	3.59[a] (3.3)[b]

[a]Best device performance. [b]Average device performance.

DOI: 10.1021/am506886d
ACS Appl. Mater. Interfaces 2015, 7, 2359−2366

390 nm) by varying the volume of the precursor solution (200, 300, 400, and 500 μL, respectively) containing the optimal MAI/PbI_2 ratio (1:0.75). The value of J_{SC} increased upon increasing the film thickness to 220 nm, reaching a maximum of 16.36 mA cm^{-2} (Figure 3d). Further increasing the thickness to 330 and 390 nm caused the value of J_{SC} to decrease, although the values of V_{OC} remained constant at the different thicknesses (Table 2). Using this device fabrication procedure, a film of optimal thickness would absorb more light and yield a higher current.

In a planar heterojunction architecture, perovskite film formation is thermodynamically unstable upon PEDOT:PSS, with the changes in morphology being driven mainly by minimization of surface energy during the annealing process. To observe the phenomena of film growth and coverage, we recorded SEM images (Figure 5) at each step of the optimized

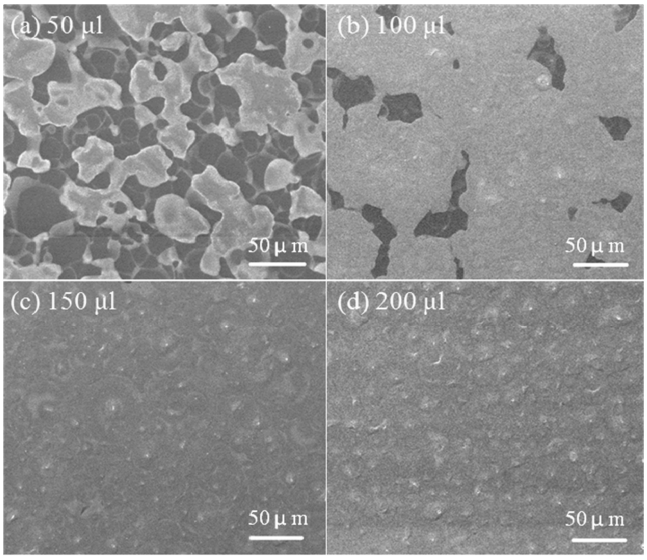

Figure 5. Top-view SEM images of perovskite films prepared through spray-coating of a precursor solution (MAI/PbI_2 ratio: 1:0.75) at volumes of (a) 50, (b) 100, (c) 150, and (d) 200 μL onto ITO/PEDOT:PSS at a substrate temperature of 50 °C, after subsequent annealing at 100 °C for 1 h.

conditions, namely, spraying 50 μL of the precursor solution (MAI/PbI_2 ratio: 1:0.75) onto the ITO/PEDOT:PSS substrate at a substrate temperature of 50 °C, with postspray annealing at a temperature of 100 °C. The morphology of the sample sprayed at a volume of 50 μL revealed partial coverage with a number of islands; we attribute this behavior to an insufficient volume of precursor solution to cover the entire area. Notably, in one case, the micro droplets that fell onto the substrate remained at the same location without migrating. Interestingly, by increasing the volume of precursor solution to 100 μL, the film exhibited greater coverage through the connecting of islands through layer-by-layer growth, resulting in a continuous film with low dewetting. Solvents having high boiling points can result in large-area variations in thickness or dewetting of cast films as a result of the necessity for prolonged drying times.[24] We did not observe such behavior during the spray-coating process because the solidification process occurred immediately when the droplets reached the substrate heated at the optimal substrate temperature. The variations in thickness occurred mainly from accumulation of solvent at one particular point; it could be avoided by fine-tuning the nozzle size. The dewetting of the cast film was easy to control by varying the substrate temperature and the postdeposition annealing temperature. By following these key factors, we sprayed the precursor solution at higher volumes (150 and 200 μL) to connect the islands and cover the entire substrate. To achieve coverage over the entire film, the nozzle size, the precursor concentration, the spray deposition temperature, and the postspray annealing temperature should all be optimized.

Figure 6 displays the performance of our best device as well as the statistical device performance of 50 devices prepared from five batches. The optimal device displayed the highest PCE (10.2%) with a J_{SC} value of 17.3 mA cm^{-2}, a V_{OC} value of 0.93 V, and an FF value of 0.63 (Figure 6a). To confirm the reproducibility of this device performance, and to disprove that the high boiling point solvent resulted in the formation of large-area variations in thickness or dewetting as a result of prolonged drying times, we fabricated 50 devices for a statistical analysis. Figure 6c–f reveals that 85% of the devices have efficiencies of greater than 8.3%, with an average efficiency of approximately 9.2%, with J_{SC} values greater than 14.5 mA cm^{-2}, V_{OC} values greater than 0.9 V, and FF values greater than 0.6. In addition, the average PCE device was measured to observe hysteresis as shown in Figure 6b; the subjected device shows negligible hysteresis in forward and reverse scan. To confirm the advantages of spray-coating, we fabricated large-area (60 and 342 mm^2) devices and determined their performance (Figure 7, Table 3). The device having an area of 342 mm^2 exhibited a PCE of 4.66% with a J_{SC} of 15.49 mA cm^{-2}; the 60 mm^2 device had a PCE of 6.88% and a J_{SC} of 14.01 mA cm^{-2}. Although the PCE of large-area devices was lower than the optimized small-area unit cell, further device optimization and the serial connection of individual cells with a suitably size electrode pattern can enhance the performance. The main advantage of this work was using the simple and cheap airbrush pen for fabricating the efficient perovskite solar cells. Moreover, the systematically studied film growth and coverage at various conditions, such as thickness, ratio, substrate temperature during spray coating, and post annealing temperature were also advantageous. Finally, the devices with areas of 60 mm^2 and 342 mm^2 were demonstrated. This indicates that the spray coating is a promising method for mass production.

CONCLUSION

To encourage the preparation of perovskite photovoltaic devices through commercial roll-to-roll processing, here we have fabricated lead halide perovskite thin films through spray-coating using a cheap and simple airbrush pen. A precursor solution containing an MAI/PbI_2 ratio of 1:0.75 provided the best device performance and the highest film coverage. To study the perovskite film coverage and formation, we recorded SEM images of films prepared at different volumes, substrate temperatures, and postspray annealing temperatures. At a spray volume of 150 μL, the film covered the entire substrate when the substrate temperature was 50 °C and the postspray annealing temperature was 100 °C. The optimal device exhibited a PCE of 10.2%; the average device performance was approximately 9.2%. In addition, lead halide perovskite solar cells having large active areas of 60 and 342 mm^2 achieved attractive PCEs of 6.88 and 4.66%, respectively.

DOI: 10.1021/am506886d
ACS Appl. Mater. Interfaces 2015, 7, 2359–2366

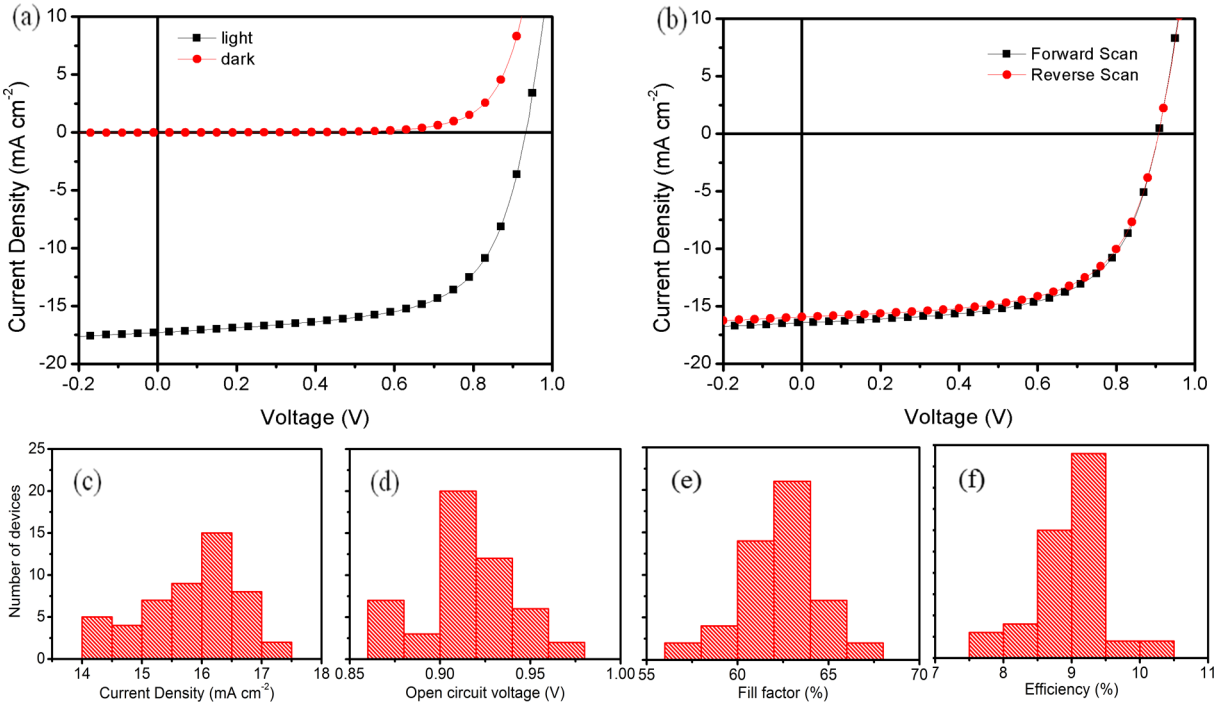

Figure 6. Current density−voltage curve of (a) optimal device, (b) forward and reverse scan of average PCE device, and (c−f) statistical device performances of more than 50 devices from five batches.

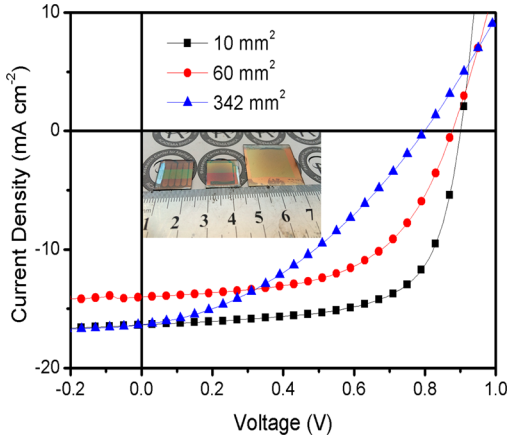

Figure 7. Current density−voltage characteristics of devices incorporating perovskite films of various areas, prepared from a precursor solution containing an MAI/PbI_2 ratio of 1:0.75.

Table 3. Photovoltaic Performance Parameters of Devices Having Different Device Areas

area [mm^2]	current I_{SC} [mA]	J_{SC} [mA cm^{-2}]	V_{OC} [mV]	FF	PCE [%]
10	1.64	16.36	0.90	0.65	9.70
60	8.41	14.01	0.88	0.56	6.88
342	52.97	15.49	0.8	0.38	4.66

■ ASSOCIATED CONTENT

Supporting Information

Dark current densities of devices incorporating perovskite films prepared at various precursor (MAI/PbI_2) ratios. Top-view SEM images of perovskite films prepared at different substrate temperatures. Absorption spectra, XRD patterns, and top-view SEM images of perovskite films prepared at different annealing temperatures. This material is available free of charge via the Internet at http://pubs.acs.org.

■ AUTHOR INFORMATION

Corresponding Author

*Phone: 886-2-2787-3183. Fax: 886-2-2787-3122. E-mail: gchu@gate.sinica.edu.tw.

Notes

The authors declare no competing financial interest.

■ ACKNOWLEDGMENTS

M.R. and K.M.B. contributed equally to this work. C.-W.C. thanks the Ministry of Science and Technology (MOST), Taiwan (102-2221-E-001-029-MY2), and Academia Sinica, Taiwan (Career Development Award No. 103-CDA-M01), for financial support.

■ REFERENCES

(1) Grätzel, M.; Janssen, R. A. J.; Mitzi, D. B.; Sargent, E. H. Materials Interface Engineering for Solution-Processed Photovoltaics. *Nature* **2012**, *488*, 304−312.

(2) Krebs, F. C. Fabrication and Processing of Polymer Solar Cells: A Review of Printing and Coating Techniques. *Sol. Energy Mater. Sol. Cells* **2009**, *93*, 394−412.

(3) Barkhouse, D. A. R.; Gunawan, O.; Gokmen, T.; Todorov, T. K.; Mitzi, D. B. Device Charact -eristics of a 10.1% Hydrazine-Processed $Cu_2ZnSn(Se,S)_4$ Solar Cell. *Prog. Photovoltaics* **2012**, *20*, 6−11.

(4) Todorov, T. K.; Gunawan, O.; Gokmen, T.; Mitzi, D. B. Solution-Processed Cu(In,Ga)$(S,S e)_2$ Absorber Yielding a 15.2% Efficient Solar Cell. *Prog. Photovoltaics* **2013**, *21*, 82−87.

(5) Wang, Z.; Wang, H.; Liang, M.; Tan, Y.; Cheng, F.; Sun, Z.; Xue, S. Judicious Design of Indoline Chromophores for High-Efficiency Iodine-Free Dye-Sensitized Solar Cells. *ACS Appl. Mater. Interfaces* **2014**, *6*, 5768−5778.

(6) Zhou, J.; Zuo, Y.; Wan, X.; Long, G.; Zhang, Q.; Ni, W.; Liu, Y.; Li, Z.; He, G.; Li, C.; Kan, B.; Li, M.; Chen, Y. Solution-Processed and

DOI: 10.1021/am506886d
ACS Appl. Mater. Interfaces 2015, 7, 2359−2366

High-Performance Organic Solar Cells Using Small Molecules with a Benzodithiophene Unit. *J. Am. Chem. Soc.* **2013**, *135*, 8484−8487.
(7) Liu, Y.; Chen, C.-C.; Hong, Z.; Gao, J.; Yang, Y.-M.; Zhou, H.; Dou, L.; Li, G.; Yang, Y. Solution-Processed Small-Molecule Solar Cells: Breaking the 10% Power Conversion Efficiency. *Sci. Rep.* **2013**, *3*, 3356:1−3356:1.
(8) Lu, L.; Yu, L. Understanding Low Bandgap Polymer PTB7 and Optimizing Polymer Solar Cells Based on It. *Adv. Mater.* **2014**, *26*, 4413−4430.
(9) Stranks, S.-D.; Eperon, G.-E.; Grancini, G.; Menelaou, C.; Alcocer, M.-J. P.; Leijtens, T.; Herz, L.-M.; Petrozza, A.; Snaith, H.-J. Electron-Hole Diffusion Lengths Exceeding 1 Micrometer in an Organometal Trihalide Perovskite Absorber. *Science* **2013**, *342*, 341−344.
(10) Kim, H.; Lee, C.; Im, J.; Lee, K.; Moehl, T.; Marchioro, A.; Moon, S.; Humphry-Baker, R.; Yum, J.; Moser, J. E.; Grätzel, M.; Park, N. Lead Iodide Perovskite Sensitized All-Solid-State Submicron Thin Film Mesoscopic Solar Cell with Efficiency Exceeding 9%. *Sci. Rep.* **2012**, *2* (59), 1:1−591:7.
(11) Laban, W. A.; Etgar, L. Depleted Hole Conductor-Free Lead Halide Iodide Heterojunction Solar Cells. *Energy Environ. Sci.* **2013**, *6*, 3249−3253.
(12) Etgar, L.; Gao, P.; Xue, Z.; Peng, Q.; Chandiran, A. K.; Liu, B.; Nazeeruddin, M. K.; Grätzel, M. Mesoscopic $CH_3NH_3PbI_3/TiO_2$ Heterojunction Solar Cells. *J. Am. Chem. Soc.* **2012**, *134*, 17396−17399.
(13) Shi, J.; Luo, Y.; Wei, H.; Luo, J.; Dong, J.; Lv, S.; Xiao, J.; Xu, Y.; Zhu, L.; Xu, X.; Wu, H.; Li, D. Meng' Q. Modified Two-Step Deposition Method for High-Efficiency $TiO_2/CH_3NH_3PbI_3$ Heterojunction Solar Cells. *ACS Appl. Mater. Interfaces* **2014**, *6*, 9711−9718.
(14) Lee, M. M.; Teuscher, J.; Miyasaka, T.; Murakami, T. N.; Snaith, H. J. Efficient Hybrid Solar Cells Based on Meso-Superstructured Organometal Halide Perovskites. *Science* **2012**, *338*, 643−647.
(15) Ke, W.; Fang, G.; Wang, J.; Qin, P.; Tao, H.; Lei, H.; Liu, Q.; Dai, X.; Zhao, X. Perovskite Solar Cell with an Efficient TiO2 Compact Film. *ACS Appl. Mater. Interfaces* **2014**, *6*, 15959−15965.
(16) Ito, S.; Tanaka, S.; Manabe, K.; Nishino, H. Effects of Surface Blocking Layer of Sb_2S_3 on Nanocrystalline TiO_2 for $CH_3NH_3PbI_3$ Perovskite Solar Cells. *J. Phys. Chem. C* **2014**, *118* (169), 95−17000.
(17) Jeng, J. Y.; Chiang, Y. F.; Lee, M. H.; Peng, S. R.; Guo, T. F.; Chen, P.; Wen, T. C. $CH_3N\ H_3PbI_3$ Perovskite/Fullerene Planar-Heterojunction Hybrid Solar Cells. *Adv. Mater.* **2013**, *25*, 3727−1732.
(18) Sun, S. Y.; Salim, T.; Mathews, N.; Duchamp, M.; Boothroyd, C.; Xing, G.; Sum, T. C.; Lam, Y. M. The Origin of High Efficiency in Low-Temperature Solution-Processable Bilayer Organometal Halide Hybrid Solar Cells. *Energy Environ. Sci.* **2014**, *7*, 399−407.
(19) You, J.; Hong, Z.; Yang, Y. M.; Chen, Q.; Cai, M.; Song, T.-B.; Chen, C.-C.; Lu, S.; Liu, Y.; Zhou, H.; Yang, Y. Low-Temperature Solution-Processed Perovskite Solar Cells with High Efficiency and Flexibility. *ACS Nano* **2014**, *8*, 1674−1680.
(20) Zhang, H.; Azimi, H.; Hou, Y.; Ameri, T.; Przybilla, T.; Spiecker, E.; Kraft, M.; Scherf, U.; Brabec, C. J. Improved High-Efficiency Perovskite Planar Heterojunction Solar Cells via Incorp -oration of a Polyelectrolyte Interlayer. *Chem. Mater.* **2014**, *26*, 5190−5193.
(21) Kim, H.-B.; Choi, H.; Jeong, J.; Kim, S.; Walker, B.; Song, S.; Kim, J.-Y. Mixed Solvents for the Optimization of Morphology in Solution-Processed, Inverted-Type Perovskite/Fullerene Hybrid Solar Cells. *Nanoscale* **2014**, *6*, 6679−6683.
(22) Hsu, H.-L.; Chen, C.-P.; Chang, J.-Y.; Yuab, Y.-Y.; Shen, Y.-K. Two-Step Thermal Anneali -ng Improves the Morphology of Spin-Coated Films for Highly Efficient Perovskite Hybrid Photovoltaics. *Nanoscale* **2014**, *6*, 1028−10288.
(23) Licari, J. J. *Coating Materials for Electronic Applications—Polymers, Processes, Reliability, Testing,* 1st ed; Noyes Publications/William Andrew: New York, 2003.
(24) Barrows, A.-T.; Pearson, A.-J.; Kwak, C.; Dunbar, A.-D. F.; Buckley, A.-R.; Lidzey, D.-G. Efficient Planar Heterojunction Mixed-Halide Perovskite Solar Cells Deposited via Spray- Deposition. *Energy Environ. Sci.* **2014**, *7*, 2944−2950.
(25) Wang, Q.; Shao, Y.; Dong, Q.; Xiao, Z.; Yuan, Y.; Huang, J. Large Fill-Factor Bilayer Iodine Perovskite Solar Cells Fabricated by a Low-Temperature Solution-Process. *Energy Environ. Sci.* **2014**, *7*, 2359−2365.
(26) Xiao, Z.; Bi, C.; Shao, Y.; Dong, Q.; Wang, Q.; Yuan, Y.; Wang, C.; Gao, Y.; Huang, J. Efficient, High Yield Perovskite Photovoltaic Devices Grown by Interdiffusion of Solution-Processed Precursor Stacking Layers. *Energy Environ. Sci.* **2014**, *7*, 2619−2623.
(27) Perez, M.-D.; Borek, C.; Forrest, S.-R.; Thompson, M.-E. Molecular and Morphological Influences on the Open Circuit Voltages of Organic Photovoltaic Devices. *J. Am. Chem. Soc.* **2009**, *131*, 9281−9286.
(28) Thompson, C. V. Solid-State Dewetting of Thin Films. *Annu. Rev. Mater. Res.* **2012**, *42*, 399−434.

DOI: 10.1021/am506886d
ACS Appl. Mater. Interfaces 2015, 7, 2359−2366